

ALICE EXPERIMENTAL RESULTS*

ADAM MATYJA

on behalf of the ALICE Collaboration

The Henryk Niewodniczański Institute of Nuclear Physics PAN
Radzikowskiego 152, Kraków, Poland*(Received April 28, 2014)*

We present selected results devoted to the global properties of dense matter produced in the Pb–Pb collisions at $\sqrt{s_{NN}} = 2.76$ TeV measured by the ALICE Collaboration. Several first results on p –Pb collisions at $\sqrt{s_{NN}} = 5.02$ TeV related to the double ridge structure, identified transverse momentum particle spectra and baryon-to-meson ratio are briefly reviewed. Nuclear modification factor for charged hadrons, identified light and heavy flavors are discussed together with the studies on reconstructed jets.

DOI:10.5506/APhysPolB.45.1521

PACS numbers: 25.75.–q

1. Introduction

The ALICE [1] experiment at the LHC [2] is designed to study dense and hot matter created in the ultra-relativistic Pb–Pb collisions at the highest energy densities available up to now. Under conditions of very high energy density, much higher than nuclear densities, the new state of matter known as the Quark–Gluon Plasma (QGP) is supposed to be created [3]. Moreover, the QGP state is believed to appear at the very early Universe up to a couple of 10^{-6} s just after the Big Bang.

The ALICE detector contains several sub-detectors made in almost all known techniques. The Inner Tracking System (ITS) which is surrounding the beam pipe is a 6-layer silicon detector made in 3 different techniques: pixel (SPD), drift (SDD) and strips (SSD). The Silicon Pixel Detector is responsible for the vertex determination which allows to distinguish charm and beauty particles. It is also commonly used as a trigger. The main tracking device is the large gaseous Time Projection Chamber detector, which together with ITS builds up the Central Tracking System (CTS). CTS covers

* Presented at the Cracow Epiphany Conference on the Physics at the LHC, Kraków, Poland, January 8–10, 2014.

the whole azimuth and rapidity region $|\eta| < 0.9$ ¹. Apart from tracking, CTS is used for particle identification (PID). The other sub-detectors like Transition Radiation Detector (TRD), Time Of Flight (TOF), High Momentum PID (HMPID) supports CTS in differentiation of various particle species. There are two electromagnetic calorimeters within the ALICE experiment. The Photon Spectrometer (PHOS) is a high granularity detector with a small acceptance $|\eta| < 0.13$ and $260^\circ < \phi < 320^\circ$. The PHOS is located at the bottom cradle of the ALICE detector at a radius ~ 460 cm. The Electromagnetic Calorimeter (EMCal) is placed opposite to the PHOS. It covers 100 degrees in azimuth direction ϕ . In longitudinal direction, it has ~ 700 cm of length, covering $|\eta| < 0.7$. EMCal is placed 430–440 cm out of the Interaction Point in the radial direction. The dedicated Muon Arm in the forward region $-4 < \eta < -2.5$ allows to study muon physics. The VZERO (V0) hodoscope together with Zero Degree Calorimeter (ZDC) are used for centrality determination [4]. The detailed description of the ALICE detector is provided elsewhere [1].

The ALICE experiment collected $\sim 10 \mu\text{b}^{-1}$ and $\sim 100 \mu\text{b}^{-1}$ of Pb–Pb data at $\sqrt{s_{NN}} = 2.76$ TeV in 2010 and 2011, respectively. At the end of the year 2012, ALICE collected a small pilot p –Pb sample of $\sim 0.8 \mu\text{b}^{-1}$ at $\sqrt{s_{NN}} = 5.02$ TeV. The greater sample $\sim 30 \text{nb}^{-1}$ of p –Pb at $\sqrt{s_{NN}} = 5.02$ TeV came in 2013. Since the beginning of LHC activity, ALICE collected also pp data with various energies $\sqrt{s} = 0.9, 2.36, 2.76, 7, 8$ TeV. The pp data are mainly used as a reference for hot and dense matter studies in Pb–Pb. p –Pb data are used for cold nuclear matter effect studies and also as a reference for Pb–Pb.

In the next sections, we present a small sample of the ALICE results. Section 2 is devoted to the analyses probing the global properties of the dense matter created in Pb–Pb collisions. The recent results obtained in p –Pb analyses are presented in Section 3. In Section 4 we present the experimental results related to the jet quenching phenomenon in various systems based on the ALICE data samples. Finally, we summarize in Section 5.

2. Global properties of dense matter in Pb–Pb collisions

In this section, results of the analyses devoted to the basic features of the system produced in the Pb–Pb collisions are presented. The average charged-particle multiplicity density at mid-rapidity in Pb–Pb collisions at a center-of-mass energy per nucleon pair $\sqrt{s_{NN}} = 2.76$ TeV is shown in Fig. 1. The measured density of primary charged particles at mid-rapidity normalized per participant pair $dN_{\text{ch}}/d\eta/(0.5\langle N_{\text{part}} \rangle) = 8.3 \pm 0.4(\text{syst.})$ is larger by factor 2.2 compared to the RHIC data at $\sqrt{s_{NN}} = 0.2$ TeV for Au–Au

¹ $\eta = -\ln \tan(\theta/2)$.

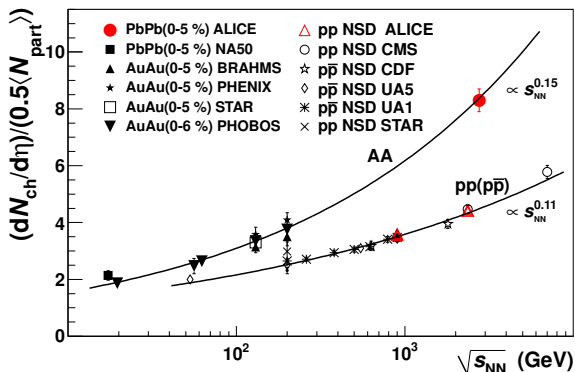


Fig. 1. Charged-particle pseudorapidity density per participant pair for central (0–5%) Pb–Pb collisions compared to other measurements with a different energy and a different colliding system.

collisions. It corresponds to an initial energy density of $\sim 15 \text{ GeV}/\text{fm}^3$ which is approximately 3 times larger than at RHIC. The particle density at mid-rapidity is also found to be a factor 1.9 higher than that for pp and $p\bar{p}$ collisions at similar energies. The energy dependence is steeper for heavy ion collisions than for pp or $p\bar{p}$ and it is not logarithmic.

The size of the system at freeze-out can be determined via femtoscopy of identical charged pions (Fig. 2). The volume of the system is measured to be $(2\pi)^{3/2}R_{\text{out}}R_{\text{size}}R_{\text{long}} \sim 5000 \text{ fm}^3$ [6] which is twice larger than measured at RHIC. The lifetime of the system from the collision to freeze-out, τ_f , extracted from the R_{long} exceeds $10 \text{ fm}/c$, which is 20% longer than at RHIC.

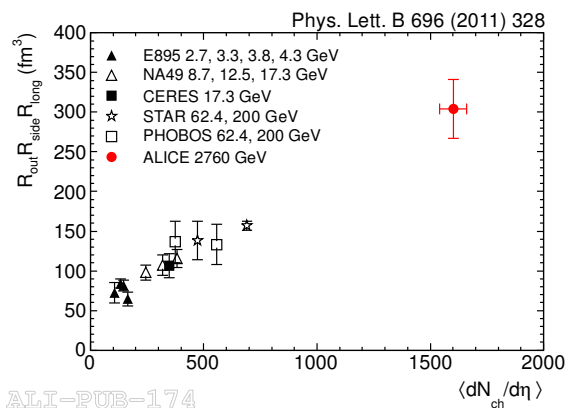


Fig. 2. Product of the three pion HBT radii in Pb–Pb collisions compared to those obtained for central gold and lead collisions at lower energies at the AGS, SPS and RHIC.

The direct photon spectrum for 0–40% most central Pb–Pb collisions [7] is shown in Fig. 3. The result agrees with NLO pQCD prediction at higher values of transverse momentum. The inverse slope parameter extracted from the exponential fit at lower p_T values, $T_{\text{LHC}} = 304 \pm 51$ MeV, indicates that the initial temperature of the medium produced in collisions is well above the critical temperature of the phase transition to QGP, $T_C \sim 170$ MeV, predicted by lattice QCD calculations [3]. In comparison, the PHENIX experiment also measured the inverse slope parameter from the photon spectrum for 0–20% Au–Au collisions at $\sqrt{s_{NN}} = 200$ GeV, $T_{\text{RHIC}} = 221 \pm 19(\text{stat.}) \pm 19(\text{syst.})$ MeV [8]. Both RHIC and LHC results prefer hydrodynamic models with initial temperature $T_{\text{init}} \sim 500\text{--}600$ MeV.

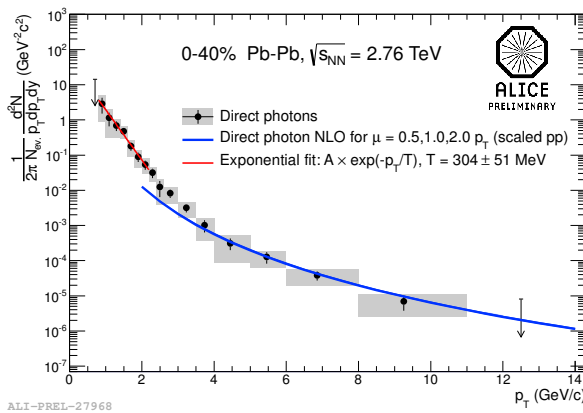
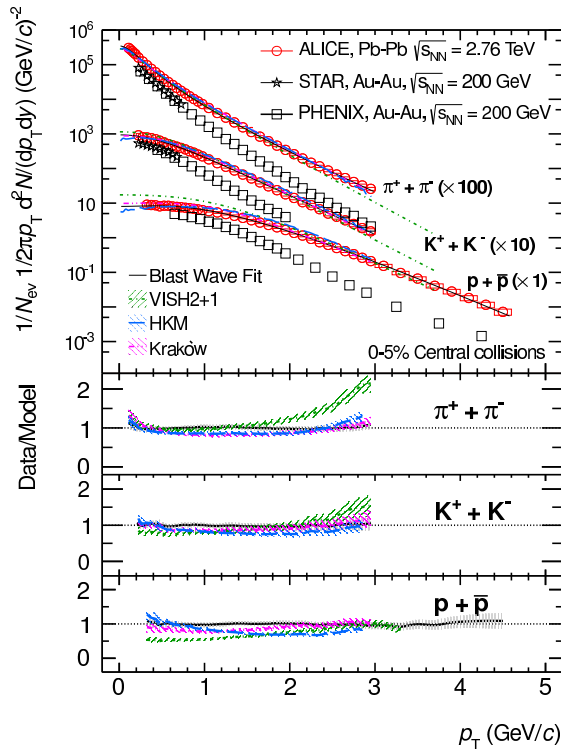


Fig. 3. Direct photon spectrum for 0–40% most central Pb–Pb collisions with NLO pQCD predictions ($2 < p_T < 14$ GeV/c) and an exponential fit ($0.8 < p_T < 2.2$ GeV/c).

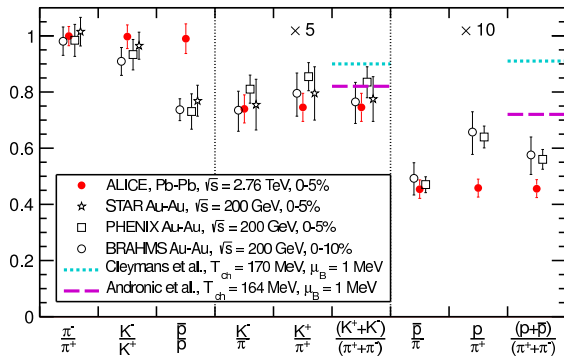
The p_T spectra of protons, pions and kaons measured in central Pb–Pb collisions [9] are shown in Fig. 4. Spectra are well described by the blast wave fits [10] with a collective radial flow velocity $\langle \beta_T \rangle = 0.65 \pm 0.02$ (which is 10% larger than at RHIC) and a kinetic freeze-out temperature of $T_{\text{kin}} = 95 \pm 10$ MeV. Data are in a good agreement with hydrodynamic predictions. The antiparticle-to-particle ratios, shown in Fig. 5, are all unity at the LHC energies, in contrast to RHIC energy, where the \bar{p}/p ratio is well below unity. The ratios kaon to pion and proton to pion are also shown. The observed particle abundances from RHIC were described well by thermal models. Predictions for higher energies [11] describe data relatively good, however there are tensions in proton sector (see the right pannel of Fig. 5).

The spatial anisotropy of non-central Pb–Pb collisions leads to strong pressure gradients. It is reflected in the momentum anisotropy. The effect is quantified by the Fourier expansion of the angular particle distributions.



ALI-PUB-45331

Fig. 4. Spectra of transverse momentum of sum of positive and negative particles fitted individually with a blast wave function, compared to RHIC data and hydrodynamic models.



ALI-PUB-45363

Fig. 5. Particle ratios at mid-rapidity compared to RHIC results and predictions from the thermal models.

The integrated second Fourier coefficient, v_2 (the elliptic flow), is measured at mid-rapidity to be around 0.065 for 20–30% Pb–Pb collisions at $\sqrt{s_{NN}} = 2.76$ TeV [12]. It increases by about 30% from RHIC to LHC energy. Some

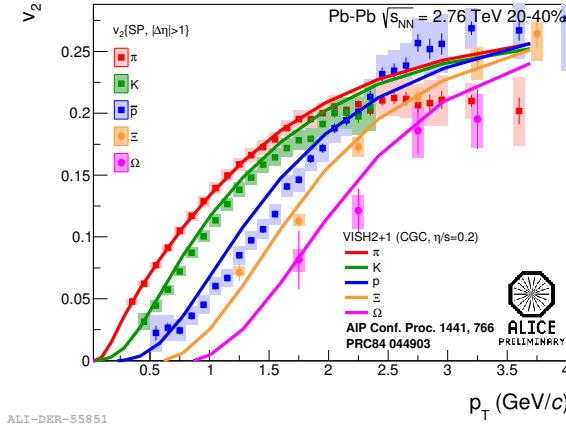


Fig. 6. v_2 of identified hadrons *versus* p_T in Pb–Pb collisions.

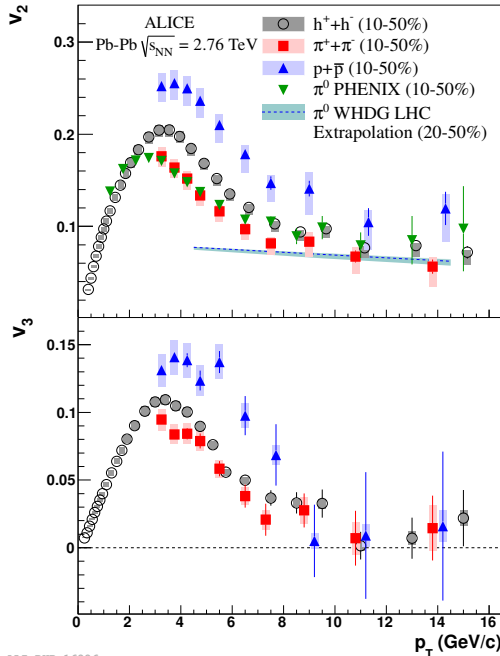


Fig. 7. The elliptic (v_2) and triangular (v_3) flow *versus* p_T for unidentified charged hadrons, pions and (anti-)protons compared to RHIC data and WHDG model calculations.

hydro models [13] are preferred by that fact. The detailed studies of v_2 for identified particles show a mass ordering at low p_T [14], followed by a hydrodynamic description (Fig. 6). A particle dependence of the elliptic flow persists up to $p_T \approx 8$ GeV/ c [15]. Both v_2 and v_3 are above zero at least up to 10 GeV/ c in p_T (Fig. 7). Elliptic flow for D mesons, shown in Fig. 8, is similar in magnitude to that observed for charged hadrons [16]. Moreover, it is significantly greater than zero in $2 < p_T < 6$ GeV/ c range. It suggests that charm quarks also take part in the collective expansion of the medium.

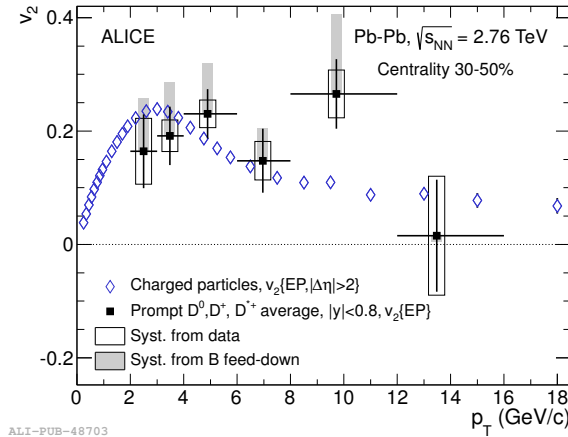


Fig. 8. Average v_2 of D^0 , D^+ and D^{*+} mesons versus p_T compared to charged particle flow.

3. Properties of matter produced in p -Pb collisions

In this section, we focus on three subjects. The observed double ridge structure in different analyses is described at first. Then identified particle transverse momentum spectra are shown. Finally, we present the baryon to meson ratio.

The associated yield per trigger particle for di-hadron correlations with $2 < p_{T,\text{trig}} < 4$ GeV/ c is presented in Fig. 9 for the low multiplicity class (60–100%) (left panel) and for the high multiplicity class (0–20%) (right panel). The well seen peak near $\Delta\phi \sim 0$ and $\Delta\eta \sim 0$ (near side) is coming from the particle pairs originating from the same jet. The elongated structure near $\Delta\phi \sim \pi$ (away side) comes from back-to-back particles. An excess on near side is visible for high multiplicity events. It is similar to that observed by the CMS Collaboration [17]. In order to quantify this effect, the per trigger yield for the low multiplicity class is subtracted from the one of the high multiplicity class. It surprisingly results in a double ridge structure [18], shown in Fig. 10. The projection of Fig. 10 onto $\Delta\phi$, presented

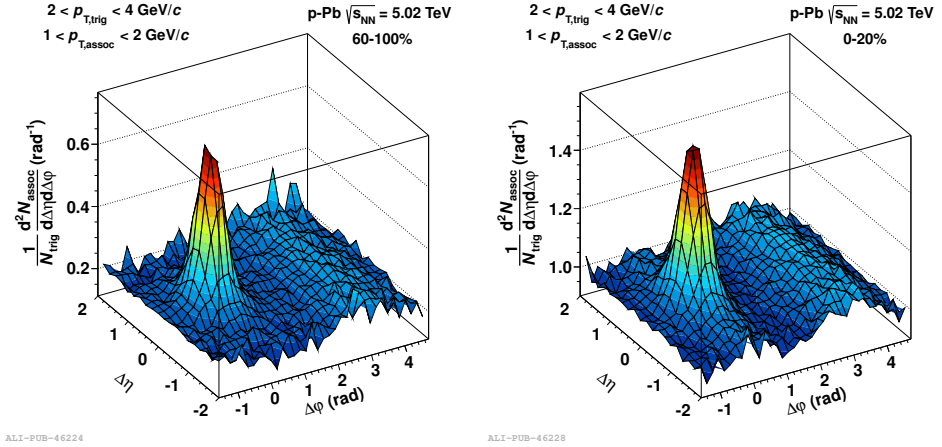


Fig. 9. Associated yield per trigger particle in $\Delta\phi$ and $\Delta\eta$ of charged particles with $2 < p_{T,\text{trig}} < 4$ GeV/c and $1 < p_{T,\text{assoc}} < 2$ GeV/c in p-Pb collisions at $\sqrt{s_{NN}} = 5.02$ GeV/c for low (left) and high (right) multiplicity classes.

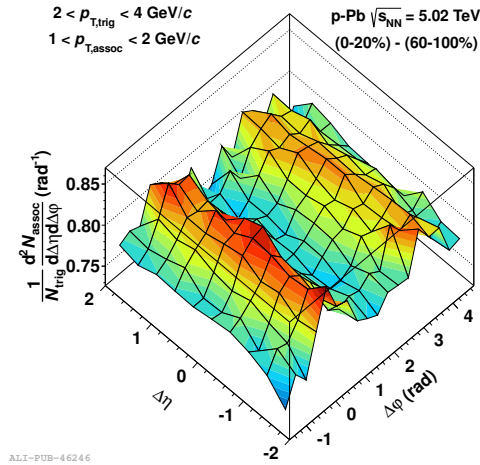
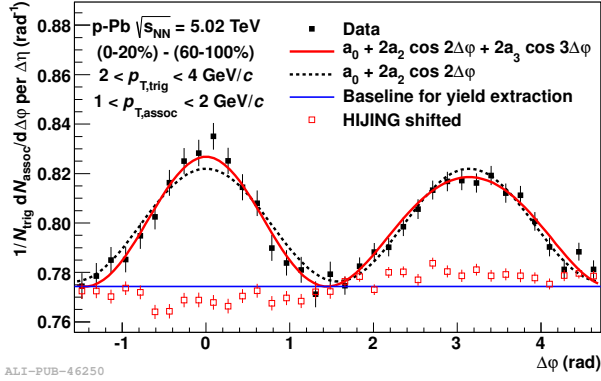


Fig. 10. Per trigger yield after subtraction of the yield for the low multiplicity class from the one of the high multiplicity class.

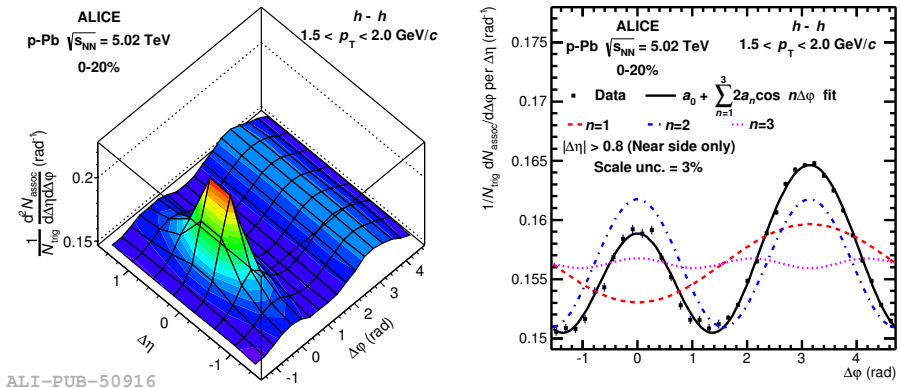
in Fig. 11, shows a clear double-modulation structure, in complete disagreement with the prediction of the HIJING event generator. The modulation observed appears to be similar to that caused by elliptic flow in Pb-Pb. The double ridge effect can be explained by long range angular correlations in the near and away side by both hydrodynamic [19] and CGC [20] models.



ALI-PUB-46250

Fig. 11. The associated per trigger yield after subtraction projected onto $\Delta\phi$. The open squares/red present HIJING Monte Carlo. Superimposed fits are denoted by solid/red and dashed/black lines. Fitted baseline is denoted by a horizontal/blue line.

More detailed studies of the double ridge structure were carried in the identified particle–hadron correlation analyses [21]. The double ridge structure is present in both pion, kaon, proton and heavy flavor decayed electron correlated with hadron analyses. The per trigger yield as a function of $\Delta\phi$ and $\Delta\eta$ for h – π correlations in 0–20% event class is shown in Fig. 12 (left panel). The projection of the left panel in Fig. 12 correlation onto $\Delta\phi$ excluding the near side jet peak averaged in $\Delta\eta$ is shown in Fig. 12 (right panel). The Fourier coefficients up to the third order are extracted from the



ALI-PUB-50916

Fig. 12. Per trigger yield as a function of $\Delta\phi$ and $\Delta\eta$ for h – π correlations in 0–20% event class (left panel) and the projection of the left panel correlation onto $\Delta\phi$ averaged over $0.8 < |\Delta\eta| < 1.6$ on the near side and $|\Delta\eta| < 1.6$ on the away side (right panel). The fit and its individual components are superimposed.

fit to $\Delta\phi$ projection. The second harmonics are drawn for h , π , K and p as a function of p_T in Fig. 13 for different multiplicity classes. v_2 increases with p_T for each particle type correlation. There is a particle type hierarchy visible, $v_2^p < v_2^K < v_2^\pi$, at low p_T . The observation is similar to measurements in Pb–Pb collisions.

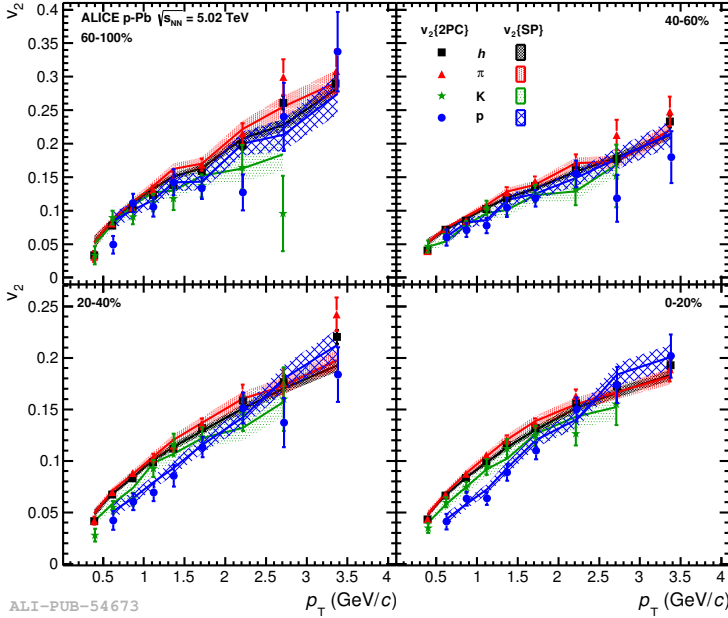


Fig. 13. The second Fourier coefficient v_2 versus p_T for charged hadrons, π , K and p for different multiplicity classes.

The ALICE Collaboration has measured particle spectra of charged pions, kaons, protons, lambdas and neutral kaons in p –Pb collisions [22]. Example spectra of pions in multiplicity classes are shown in Fig. 14. Spectra become harder with multiplicity. The effect is increased with particle mass. Particle spectra for 5–10% multiplicity class compared to various models are shown in Fig. 15. Hydrodynamic models give better description of data.

The proton to pion ratio as a function of p_T for the 0–5% and 60–80% event classes are shown in Fig. 16 for p –Pb on the left and for Pb–Pb reactions on the right panel [23]. There is a significant enhancement at $p_T \sim 3$ GeV/ c visible which disappears at large p_T . The effect is similar for both p –Pb and Pb–Pb collisions, however, the magnitude of the effect is different for two systems. The Pb–Pb result can be understood in terms of collective radial expansion and hadronization via quark recombination. The p/π ratio as a function of charged particle density $dN_{ch}/d\eta$ in three p_T ranges is shown in Fig. 17. The same exponent of power-law behavior is observed for p –Pb and for Pb–Pb collisions.

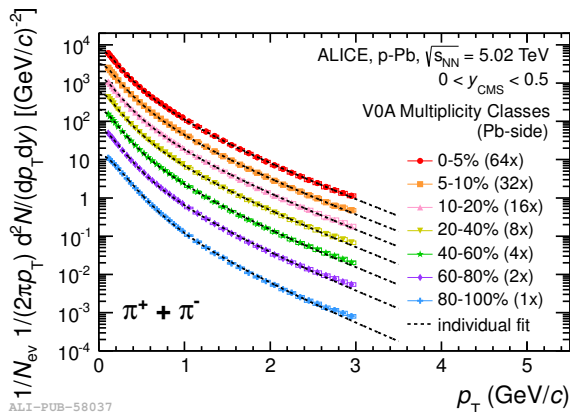


Fig. 14. Invariant yield of pions *versus* p_T for different multiplicity classes for p -Pb collisions at $\sqrt{s_{NN}} = 5.02$ TeV measured in the rapidity interval $0 < y_{CMS} < 0.5$.

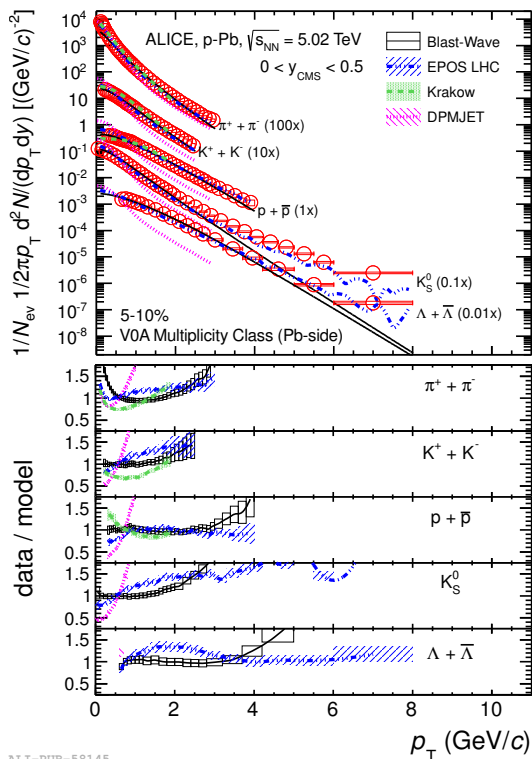
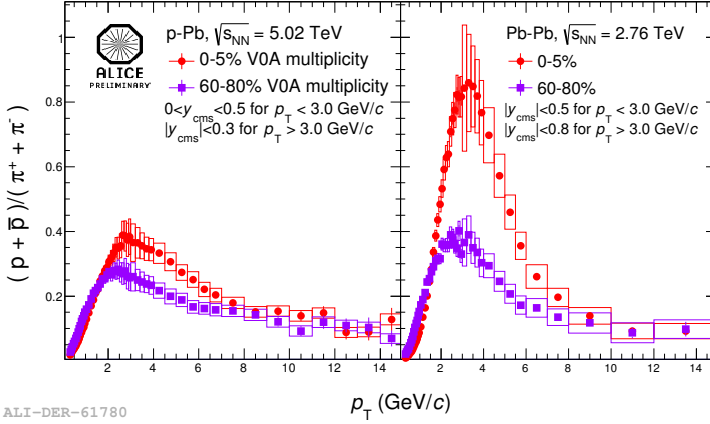
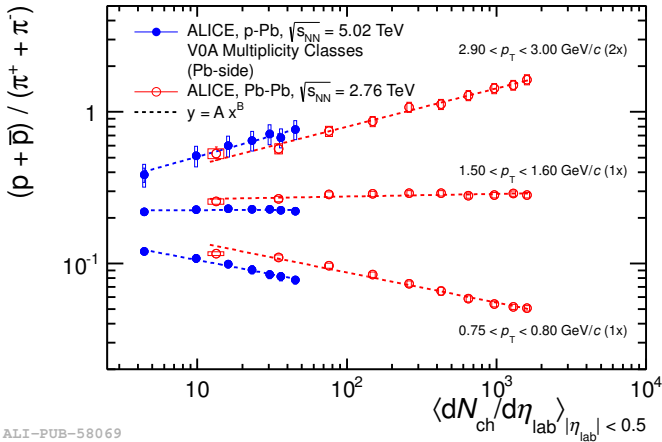


Fig. 15. Transverse momentum distribution for charged pions, kaons, protons, lambdas and neutral kaons in 5-10% multiplicity class measured in the rapidity interval $0 < y_{CMS} < 0.5$ compared to several models.



ALI-DER-61780

Fig. 16. Baryon to meson ratio for p -Pb (left) compared to Pb-Pb (right) collisions for high and low multiplicity classes.



ALI-PUB-58069

Fig. 17. p/π ratio as a function of charged particle density $dN_{ch}/d\eta$ in three p_T intervals in p -Pb and Pb-Pb collisions.

4. Jet quenching in various systems

The impact of nuclear surrounding on hard probes traversing dense matter can be justified by the nuclear modification factor

$$R_{AA}(p_T) = \frac{dN_{AA}/dp_T}{\langle N_{coll} \rangle dN_{pp}/dp_T},$$

where dN_{AA}/dp_T is number of particles emitted per event in p_T intervals for nuclear collisions, dN_{pp}/dp_T is the same but for pp collisions scaled by

number of binary nucleon–nucleon collisions N_{coll} . $R_{AA} = 1$ corresponds to AA superposition of nucleon–nucleon, while $R_{AA} < 1$ corresponds to suppression.

We present measurements on three different levels of complexity: for unidentified charged hadrons result at first, than for identified light and heavy flavored particles, and finally results for fully reconstructed jets.

Figure 18 shows nuclear modification factor of unidentified hadrons as a function of p_T for p –Pb and Pb–Pb collisions [24]. There is a strong suppression observed in central Pb–Pb events, while for p –Pb R_{AA} is consistent with unity for $p_T > 2$ GeV/ c . This indicates that the strong suppression of hadron production at high p_T in Pb–Pb is a final state effect — jet quenching in hot and dense matter. Results of R_{AA} for identified charged pions, kaons and (anti-)protons are shown in Fig. 19. There is a stronger suppression for central than for peripheral collisions. Mass ordering is visible at low p_T , while at high $p_T > 8$ GeV/ c particle are equally suppressed.

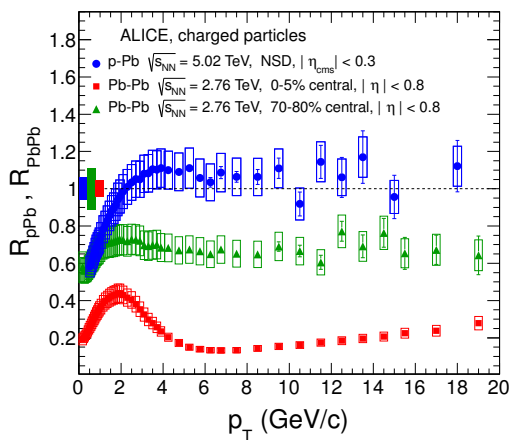


Fig. 18. Nuclear modification factor *versus* p_T in minimum bias p –Pb collisions at $\sqrt{s_{NN}} = 5.02$ TeV compared to central (0–5% centrality) and peripheral (70–80% centrality) Pb–Pb collisions at $\sqrt{s_{NN}} = 2.76$ TeV.

Studies of charm and beauty hadrons traversing QCD matter carry very important information on medium density, through the mechanisms of in-medium parton energy loss. The nuclear modification factor for D mesons in Pb–Pb collisions is shown in Fig. 20. The same pattern and magnitude, strong suppression by factor 5, is observed for all D meson species in Pb–Pb reactions. In contrast, nuclear modification factor is consistent with unity for p –Pb collisions, as shown in Fig. 21. The p –Pb result is consistent with models that include cold nuclear matter effects (color glass condensate [25] or shadowing [26]).

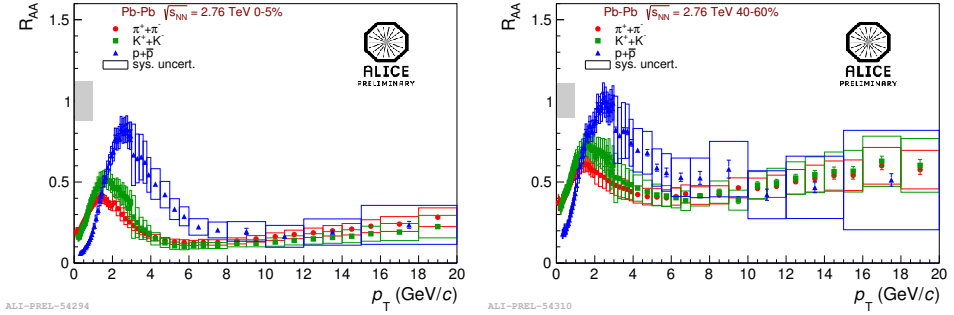


Fig. 19. Nuclear modification factor as a function of p_T for charged pions, kaons and (anti-) protons for central (0–5% centrality) (on the left) and peripheral (40–60% centrality) (on the right) Pb–Pb collisions at $\sqrt{s_{NN}} = 2.76$ TeV.

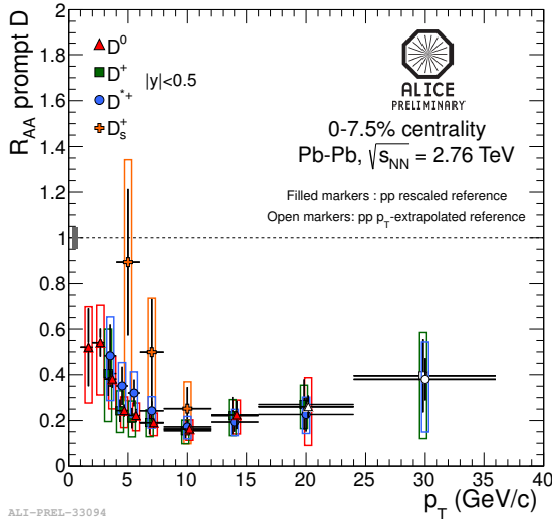


Fig. 20. Nuclear modification factor as a function of p_T for prompt D^0 , D^+ , D^{*+} and D_s^+ mesons at mid-rapidity for central (0–7.5%) Pb–Pb collisions at $\sqrt{s_{NN}} = 2.76$ TeV.

Looking at the nuclear modification factor of various mesons gives the possibility of verification of theoretical predictions on expectations from radiative energy loss. The lighter is the parton, the greater energy loss: $\Delta E_g > \Delta E_{u,d,s} > \Delta E_c > \Delta E_b$. This hierarchy can be reflected via $R_{AA}(B) > R_{AA}(D) > R_{AA}(\pi)$. The comparison of R_{AA} for D mesons and for pions in Pb–Pb collisions is shown in Fig. 22. The same order of suppression is visible. However, R_{AA} is smaller for D mesons than for non-prompt J/ψ from B mesons [27], shown in Fig. 23.

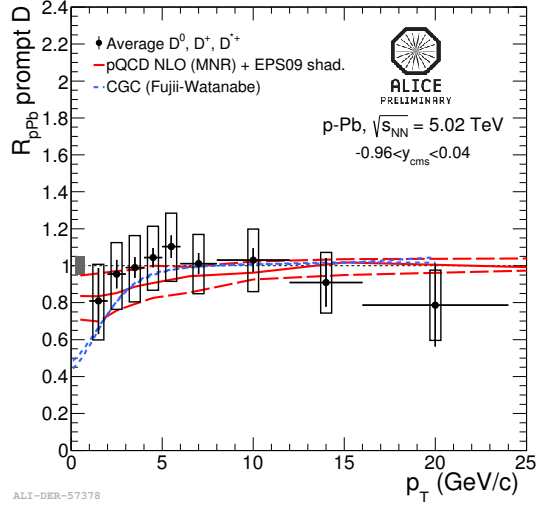


Fig. 21. Nuclear modification factor as a function of p_T for average D^0 , D^+ , D^{*+} mesons at rapidity $-0.96 < y_{CMS} < 0.04$ for p -Pb collisions at $\sqrt{s_{NN}} = 5.02$ TeV.

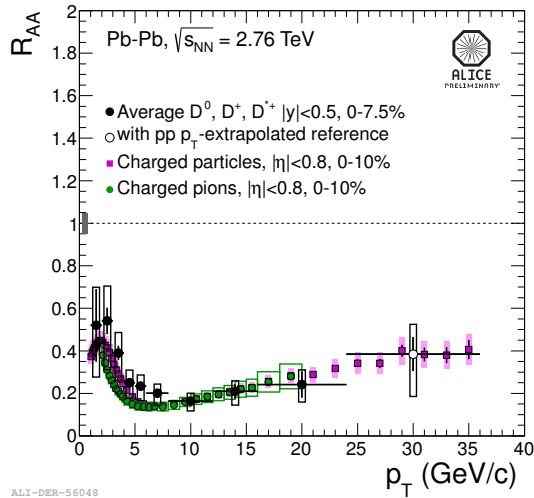


Fig. 22. The nuclear modification factor of average D^0 , D^+ , D^{*+} mesons as a function of p_T for central Pb-Pb collisions compared to charged particles and charged pions.

Suppression of quarkonium production due to the color screening was one of the first signatures of QGP [28]. At LHC energies, charmonium regeneration via the recombination of c and \bar{c} quarks can be relevant. The

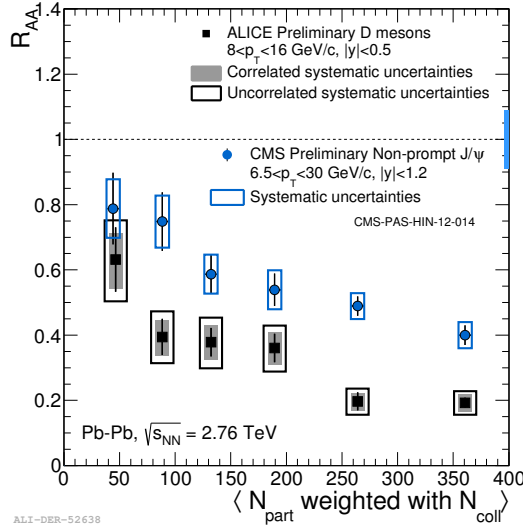


Fig. 23. The nuclear modification factor of D mesons as a function of number of participants for Pb–Pb collisions compared to CMS result on non-prompt J/ψ from B mesons.

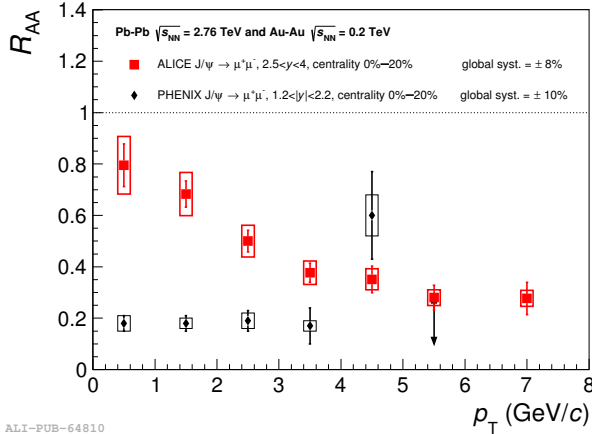


Fig. 24. The nuclear modification factor of J/ψ as a function of p_T in Pb–Pb collisions compared to PHENIX data.

R_{AA} of J/ψ mesons produced in Pb–Pb collisions has a different behavior, as a function of p_T , than at RHIC, as shown in Fig. 24. The J/ψ mesons are less suppressed at low p_T than at high p_T . ALICE also measured suppression pattern of J/ψ mesons in p –Pb collisions, shown in Fig. 25. Models containing EPS09 shadowing or coherent parton energy loss describe data well, while CGC is less favored.

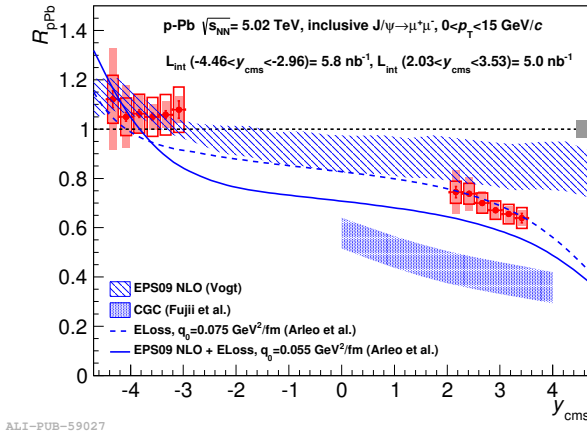


Fig. 25. The nuclear modification factor of J/ψ as a function of rapidity in p -Pb collisions compared to theoretical predictions.

How partons traversing the dense QCD matter lose their energy is one of basic questions in heavy ion collision studies. Hard scattered partons hadronise in a bunch of composed particles, which is a jet. Cross-section and fragmentation of jets was studied extensively in pp collisions. It is a good baseline for nuclear collisions. ALICE also measured the jet cross-section in pp collisions at $\sqrt{s} = 2.76$ TeV [30]. The inclusive differential jet cross-section obtained for the fully reconstructed jets with resolution parameter $R = 0.2$, is shown in Fig. 26. The ratio of jet cross-sections reconstructed with a

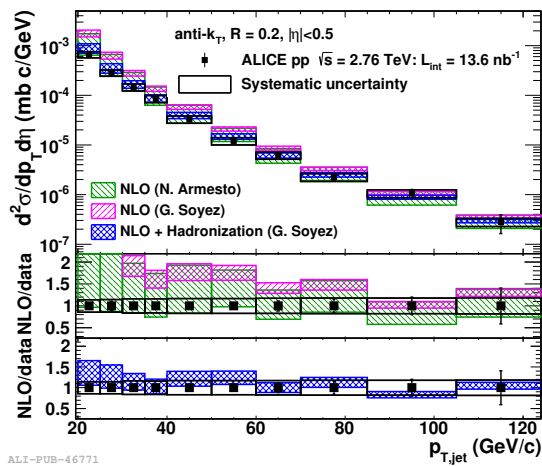


Fig. 26. The differential jet cross-section for pp collisions at $\sqrt{s} = 2.76$ TeV compared to several models.

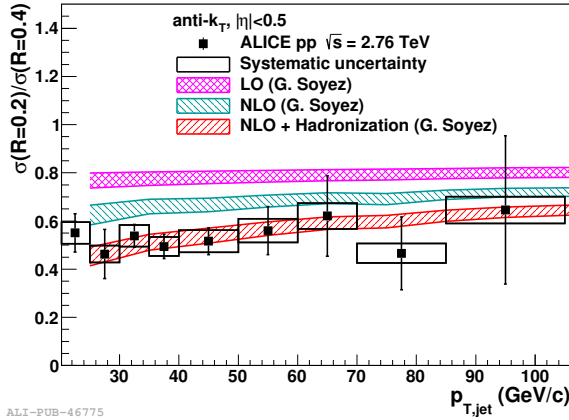


Fig. 27. Ratio of cross-sections of jets reconstructed with resolution parameter $R = 0.2$ and $R = 0.4$ as a function of $p_{T,jet}$ for pp collisions at $\sqrt{s} = 2.76$ TeV compared to model predictions.

resolution parameter (cone radius) $R = 0.2$ and $R = 0.4$ is shown in Fig. 27. This ratio which is a sensitive observable to the jet broadening is less than unity. Both the cross-section and the ratio are compared to several models. It is clearly seen that inclusion of hadronisation correction to Next-To-Leading-Order (NLO) pQCD calculation describes both spectra quite well. The nuclear modification factor for fully reconstructed jets was measured for 10% most central events in Pb–Pb collisions at $\sqrt{s_{NN}} = 2.76$ TeV [31], as shown in Fig. 28. ALICE has measured R_{AA} down to $p_T = 30$ GeV/ c , where a strong suppression is visible. The ratio of cross-sections of charged jets reconstructed with a resolution parameter $R = 0.2$ and $R = 0.3$ as a function of a transverse momentum for central (0–10%) and peripheral (50–80%) collisions at $\sqrt{s_{NN}} = 2.76$ TeV [32] is shown in Fig. 29. The ratio of jet cross-sections is compatible with fragmentation in vacuum described by Pythia. It also shows no evidence of jet shape modification in the jet core.

Finally, we present the nuclear modification factor for reconstructed charged jets in p –Pb collisions [33]. As shown in Fig. 30, the jet nuclear modification factor is consistent with unity, so there is no modification caused by any cold nuclear matter effect. Comparison with charged hadrons shows that binary scaling holds.

To check possible cold nuclear matter effects on the jet profile the jet yield ratio for two resolution parameters $R = 0.2$ and $R = 0.4$ was calculated and is shown in Fig. 31. The comparison with pp results and Pythia shows no additional effects.

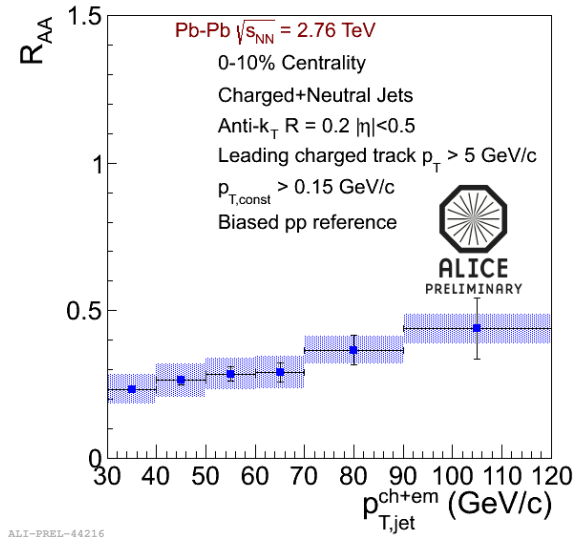


Fig. 28. Nuclear modification factor for fully reconstructed jets with resolution parameter $R = 0.2$ in central Pb–Pb collisions at $\sqrt{s_{NN}} = 2.76$ TeV.

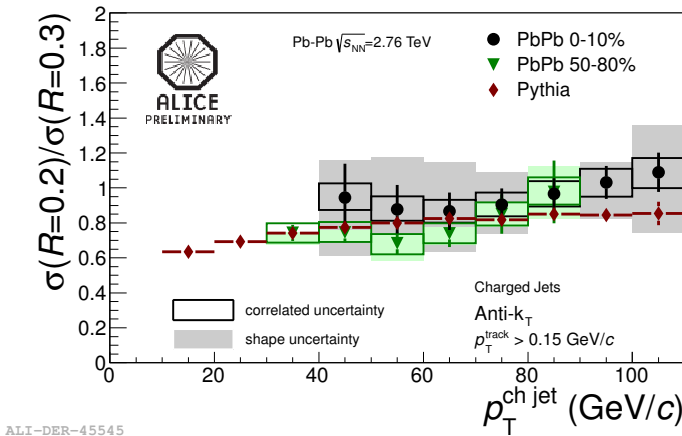


Fig. 29. Ratio of cross-sections of charged jets reconstructed with the resolution parameter $R = 0.2$ and $R = 0.3$ as a function of $p_T^{\text{ch jet}}$ for central (0–10%) and peripheral (50–80%) collisions at $\sqrt{s_{NN}} = 2.76$ TeV compared to results from the Pythia event generator.

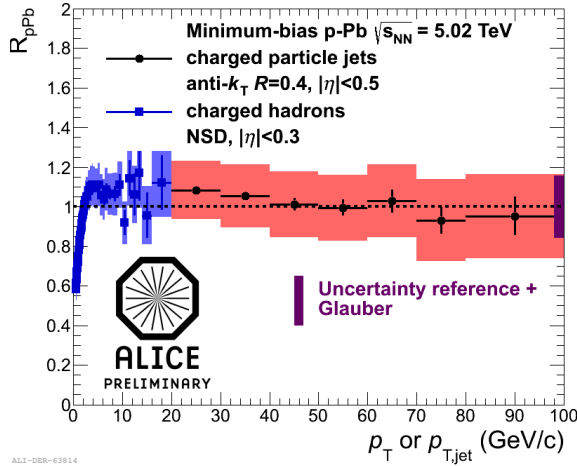


Fig. 30. Nuclear modification factor for charged reconstructed jets with resolution parameter $R = 0.4$ in p -Pb collisions at $\sqrt{s_{NN}} = 5.02$ TeV compared to charged hadrons.

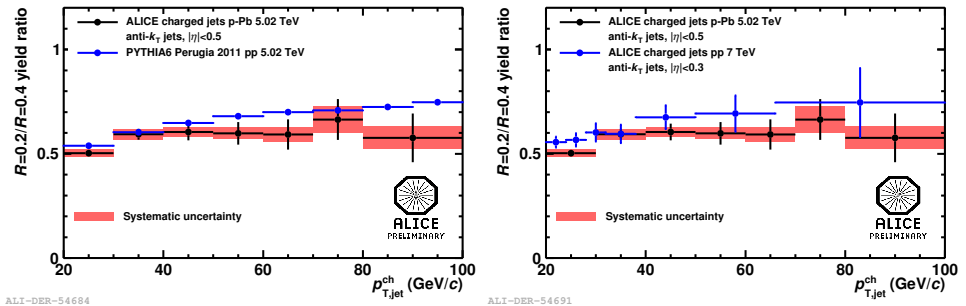


Fig. 31. Ratio of jet yield for resolution parameter $R = 0.2$ and $R = 0.4$ in p -Pb collisions at $\sqrt{s_{NN}} = 5.02$ TeV compared to left: Pythia predictions for pp collisions at $\sqrt{s} = 5.02$ TeV and right: result for charged jets in pp at $\sqrt{s} = 7$ TeV.

5. Summary

The ALICE Collaboration has obtained a large number of interesting results in both Pb-Pb, p -Pb and pp systems. This variety of results builds up a detailed picture of particle production in nucleus-nucleus, proton-nucleus and binary system. Such large number of analyses gives new ways of verification of models and incorporate new discoveries like double ridge structure in p -Pb into them.

I would like to thank the Polish National Science Center for the supporting grant DEC-2012/05/D/ST2/00855.

REFERENCES

- [1] K. Aamodt *et al.* [ALICE Collab.], *JINST* **3**, S08002 (2008).
- [2] L. Evans *et al.*, *JINST* **3**, S08001 (2008).
- [3] F. Karsch, *AIP Conf. Proc.* **842**, 20 (2006) [arXiv:hep-lat/0601013].
- [4] B. Abelev *et al.* [ALICE Collab.], *Phys. Rev.* **C88**, 044909 (2013).
- [5] K. Aamodt *et al.* [ALICE Collab.], *Phys. Rev. Lett.* **105**, 252301 (2010).
- [6] K. Aamodt *et al.* [ALICE Collab.], *Phys. Lett.* **B696**, 328 (2011).
- [7] M. Wilde [ALICE Collab.], *Nucl. Phys.* **A904–905**, 573c (2013).
- [8] A. Adare *et al.* [PHENIX Collab.], *Phys. Rev. Lett.* **104**, 132301 (2010).
- [9] B. Abelev *et al.* [ALICE Collab.], *Phys. Rev. Lett.* **109**, 252301 (2013).
- [10] E. Schnedermann *et al.*, *Phys. Rev.* **C48**, 2462 (1993).
- [11] A. Andronic, P. Braun-Munzinger, J. Stachel, *Phys. Lett.* **B673**, 142 (2009); J. Cleymans *et al.*, *Phys. Rev.* **C73**, 034903 (2006).
- [12] K. Aamodt *et al.* [ALICE Collab.], *Phys. Rev. Lett.* **105**, 252302 (2010).
- [13] G. Kestin, U.W. Heinz, *Eur. Phys. J.* **C61**, 545 (2009); T. Hirano *et al.*, *Phys. Lett.* **B636**, 299 (2006).
- [14] F. Noferini [ALICE Collab.], *Nucl. Phys.* **A904–905**, 483c (2013).
- [15] B. Abelev *et al.* [ALICE Collab.], *Phys. Lett.* **B719**, 18 (2013).
- [16] B. Abelev *et al.* [ALICE Collab.], *Phys. Rev. Lett.* **111**, 102301 (2013).
- [17] S. Chatrchyan *et al.*, *Phys. Lett.* **B718**, 795 (2013) [arXiv:1210.5482 [nucl-ex]].
- [18] B. Abelev *et al.* [ALICE Collab.], *Phys. Lett.* **B719**, 29 (2013).
- [19] P. Bozek *et al.*, *Phys. Lett.* **B718**, 1557 (2013).
- [20] K. Dustling *et al.*, *Phys. Rev.* **D87**, 094034 (2013).
- [21] B. Abelev *et al.* [ALICE Collab.], *Phys. Lett.* **B726**, 164 (2013).
- [22] B. Abelev *et al.* [ALICE Collab.], *Phys. Lett.* **B728**, 25 (2014).
- [23] B. Abelev *et al.* [ALICE Collab.], *Phys. Rev.* **C88**, 044910 (2013).
- [24] B. Abelev *et al.* [ALICE Collab.], *Phys. Rev. Lett.* **110**, 082302 (2013).
- [25] H. Fujii, K. Watanabe, *Nucl. Phys.* **A920**, 78 (2013).
- [26] K.J. Eskola, H. Paukkunen, C.A. Salgado, *J. High Energy Phys.* **0904**, 065 (2009).
- [27] CMS Collab., CMS-PAS-HIN-12-014.
- [28] T. Matsui, H. Satz, *Phys. Lett.* **B178**, 416 (1986).
- [29] B. Abelev *et al.* [ALICE Collab.], arXiv:1308.6726 [nucl-ex].
- [30] B. Abelev *et al.* [ALICE Collab.], *Phys. Lett.* **B722**, 262 (2013).
- [31] R. Reed [ALICE Collab.], arXiv:1304.5945 [nucl-ex].
- [32] B. Abelev *et al.* [ALICE Collab.], arXiv:1311.0633 [nucl-ex].
- [33] R. Haake [ALICE Collab.], arXiv:1310.3612 [nucl-ex].